frontiers in Physics

ORIGINAL RESEARCH
published: 16 June 2021
doi: 10.3389/fphy.2021.690661

Enhanced Electrochemical Property of $Li_{1.2-x}Na_xMn_{0.54}Ni_{0.13}Co_{0.13}O_2$ Cathode Material for the New Optoelectronic Devices

Yumei Gao[1]*, *Yuchong Hui*[2] *and Hang Yin*[1]

[1]College of Electron and Information, University of Electronic Science and Technology of China, Zhongshan Institute, Zhongshan, China, [2]State Key Laboratory of Electronic Thin Films and Integrated Devices, University of Electronic Science and Technology of China, Chengdu, China

The Li-rich Mn-based oxide $Li_{1.2}Mn_{0.54}Ni_{0.13}Co_{0.13}O_2$ has been extensively studied as a cathode material of the battery module for new optoelectronic devices. To improve and enhance the electrochemical performance, sodium doping is one of the effective approaches. According to the density functional theory of first-principles, the band gap, partial density of states, lithiation formation energy, electron density difference, and potential energy of electrons for $Li_{1.2-x}Na_xMn_{0.54}Ni_{0.13}Co_{0.13}O_2$ were simulated with Materials Studio, Nanodcal, and Matlab. When the sodium doping amount x = 0.10 mol, simulations show that $Li_{1.2-x}Na_xMn_{0.54}Ni_{0.13}Co_{0.13}O_2$ has a better conductivity. The potential maps of $Li_{1.2-x}Na_xMn_{0.54}Ni_{0.13}Co_{0.13}O_2$ obtained in Matlab demonstrate that the potential barrier is lower and the rate capability is enhanced after sodium doping. Results of analyses and calculations agree with the experimental result of Chaofan Yang's group. This theoretical method could be a great avenue for the investigation of the battery application of new optoelectronic devices. Also, our findings could give some theoretical guidance for the subsequent electrochemical performance study on doping in the field of lithium-ion batteries.

Keywords: density functional theory, electrochemical performance, $Li_{12-x}Na_xMn_{054}Ni_{013}Co_{013}O_2$, optoelectronic device, cathode material

OPEN ACCESS

Edited by:
Qiang Xu,
Nanyang Technological University, Singapore

Reviewed by:
Liu Wenping,
Guilin University of Electronic Technology, China
Xiang Liu,
Nanjing Tech University, China

***Correspondence:**
Yumei Gao
yumeigao5697@163.com

Specialty section:
This article was submitted to Optics and Photonics, a section of the journal Frontiers in Physics

Received: *03 April 2021*
Accepted: *18 May 2021*
Published: *16 June 2021*

Citation:
Gao Y, Hui Y and Yin H (2021) Enhanced Electrochemical Property of $Li_{1.2-x}Na_xMn_{0.54}Ni_{0.13}Co_{0.13}O_2$ Cathode Material for the New Optoelectronic Devices. Front. Phys. 9:690661. doi: 10.3389/fphy.2021.690661

INTRODUCTION

The commercial lithium-ion batteries (LIBs) have many advantages, such as their energy saving, high energy density, good cycle performance, less pollution, no memory characteristics, and rechargeable property [1]. With the rapid development of new optoelectronic devices in recent decades, LIBs have been widely applied as the stationary energy storage of the electro-optical conversion devices. Nowadays, the actual specific capacity of conventional cathode materials, such as $LiCoO_2$, $LiMnO_2$, spinel $LiMn_2O_4$, ternary lithium nickel cobalt aluminum oxide, and olivine $LiFePO_4$, is less than 160 mAh/g, but that of the anode is much higher. Commercialized cathode materials are not adequate to match the next-generation power battery. In addition, the percentage of the cathode's cost in the whole battery's cost is very high. To meet the needs of people, the low-cost cathode materials with higher energy density and discharge/charge rate capability are urgent to be explored.

The layered Li-rich Mn-based Ni–Co–Mn (NCM) ternary cathode material $xLi_2MnO_3{\cdot}(1-x)LiMO_2$ ($0 < x < 1$, M = Ni, Co, Mn, $Ni_{1/2}Mn_{1/2}$, $Ni_{1/3}Mn_{1/3}Co_{1/3}$) has attracted extensive attention

owing to its lower price and good performance. Its space group is $R\bar{3}m$, and its layered structure is α-$NaFeO_2$–type like $LiCoO_2$; their synthesis is always thought as formed by two phases: monoclinic Li_2MnO_3-layered and rhombohedral $LiMO_2$-layered moieties [2]. However, their complex crystal structure has not yet been fully realized. It is known that Co is poisonous and expensive. In Li-rich Mn-based NCM, the percentage of Co is far lower than that of Mn; thus, with the advantages of low cost and high safety, this material is superior to the commonly used cathode material. Meanwhile, for the layered structural stability influenced by the Li_2MnO_3 component, when its first charging voltage is higher than 4.5 V (vs Li^+/Li), Li and O are removed together and its theoretical capacity is up to 377 mAh/g. Therefore, the layered Li-rich Mn-based NCM is a hot candidate for the new LIBs.

Recently, the Li-rich Mn-based oxide $Li_{1.2}Mn_{0.50}Ni_{0.13}Co_{0.13}O_2$ (or $Li[Li_{0.2}Mn_{0.54}Ni_{0.13}Co_{0.13}]O_2$) has aroused increasing attraction [3, 4], and it is considered one of the most promising layered cathode materials for the new battery of optoelectronic devices and LIBs. Its discharge-specific capacity is higher than 250 mAh/g in the voltage range from 2.0 to 4.8 V at 0.1 C. Its precursors are made by sol–gel, solid phase, coprecipitation, combustion, spray pyrolysis, and molten salt synthesis [5]. However, the application of this material has trapped seriously in higher-power systems due to high first irreversible specific capacity, poor cycling stability, and low rate capability [6]. To improve the electrochemical performance of $Li_{1.2}Mn_{0.54}Ni_{0.13}Co_{0.13}O_2$, many effective approaches, such as surface modification [7, 8] and doping [9, 10], had been employed experimentally. The cycling stability and the rate capacity can be dramatically improved by coating with the La–Co–O compound [7]. Since Cs doping can alleviate structural transition from layer to spinel, the Cs-doped $Li_{1.2}Mn_{0.54}Ni_{0.13}Co_{0.13}O_2$ has a better rate capability, a higher initial Coulombic efficiency, and a restrained discharge voltage [10]. Yb doping [11], Na^+ and F^- co-doping [12], and Mg^{2+} and PO_4^{3-} dual doping [13] were taken to strengthen the electrochemical performance of $Li_{1.2}Mn_{0.54}Ni_{0.13}Co_{0.13}O_2$. The K-doped $Li_{1.2}Mn_{0.52}Ni_{0.2}Co_{0.08}O_2$ has a higher Coulombic efficiency, a larger reversible discharging capacity, and a more well-defined layered structure, which are mainly ascribable to the accommodation of bigger metal ions K^+ enlarging Li layers to facilitate the diffusion of Li^+ and stabilize the structure [14]. Sodium doping in $Li_{1.2}Mn_{0.54}Co_{0.13}Ni_{0.13}O_2$ had been extensively experimented by Chaofan Yang's group [15]; their results showed that $Li_{1.2-x}Na_xMn_{0.54}Ni_{0.13}Co_{0.13}O_2$ (or $Li_{1.0\text{-}x}Na_x[Li_{0.2}Mn_{0.54}Ni_{0.13}Co_{0.13}]O_2$) has an excellent electrochemical performance.

In parallel with these experimental efforts, the density functional theory (DFT) based on first-principles [16–19] is applied to investigate the physical and chemical mechanics of Li-ion binding and diffusion in the crystal lattice. The results of simulations and calculations can give some theoretical study directions about the relevant experiments, shorten greatly the entire period of experiments or investigations, and reduce the experimental cost [18]. Herein, in this work, $Li_{1.2-x}Na_xMn_{0.54}Ni_{0.13}Co_{0.13}O_2$ was studied theoretically with DFT by Materials Studio, Nanodcal, and Matlab. The results exhibited that the electrochemical performance of $Li_{1.2-x}Na_xMn_{0.54}Ni_{0.13}Co_{0.13}O_2$ is affected by the amount of sodium doping, and the best sodium doping in $Li_{1.2}Mn_{0.54}Ni_{0.13}Co_{0.13}O_2$, obtained by calculations, agreed with that of experiments [15].

PRINCIPLE

Density Functional Theory

DFT originates from the uniform electronic gas model, which is called the Thomas–Fermi model [16, 20]. On the assumption of no interaction between electrons, the Schrödinger equation of the electron's motion is the wave equation shown in the following:

$$-\frac{\hbar^2}{2m}\nabla^2\psi(\boldsymbol{r}) = E\psi(\boldsymbol{r}). \tag{1}$$

Based on the distribution of free electrons' energy levels at absolute zero, the electron density ρ is shown in the following equation:

$$\rho = \frac{1}{3\pi^2}\left(\frac{2m}{\hbar^2}\right)^{\frac{3}{2}}E_{\mathrm{F}}^{\frac{3}{2}}. \tag{2}$$

Here, E_{F} is the Fermi energy level, and the kinetic energy T_{e} of a single electron is shown in the following equation:

$$T_{\mathrm{e}} = \frac{3}{5}E_{\mathrm{F}}. \tag{3}$$

And the system's kinetic energy density is shown in the following equation:

$$\rho T_{\mathrm{e}} = \frac{3}{5}\frac{h^2}{2m}\left(3\pi^2\right)^{\frac{3}{2}}\rho^{\frac{5}{3}} = C_k\rho^{\frac{5}{3}}. \tag{4}$$

Considering the external field $u(\boldsymbol{r})$ of the classical Coulombic interaction between nuclei and electrons, the total energy of the electron system can be obtained as shown in the following equation:

$$E_{\mathrm{TF}}(\boldsymbol{r}) = C_k\int r^{\frac{5}{3}}\mathrm{d}r + \int r(\boldsymbol{r})u(\boldsymbol{r})\mathrm{d}r + \frac{1}{2}\int\frac{r(\boldsymbol{r})r(\boldsymbol{r}')}{|\boldsymbol{r}-\boldsymbol{r}'|}\mathrm{d}r\mathrm{d}r'. \tag{5}$$

The above equation shows the electronic systemic total energy is affected only by the electron density function $r(r)$; hence, this theory of Thomas–Fermi model is called DFT. But this model could not be used directly. Then, Hohenberg and Kohn proposed the more exact density functional method (HK theorems) [17, 21] considering the nonrelativistic, adiabatic, and single-electron approximations. In fact, the theoretical basis of DFT is HK theorems including the first theory and the second theory. According to HK theorems, when the particles' number is constant, the ground state of particles can be expressed by a variational function of energy function on the number density function of particles $\rho(\boldsymbol{r})$, and the total energy $E_v[\rho(r)]$ relevant to external potential is shown in the following equation:

$$E_v[\rho(\boldsymbol{r})] = F[\rho(\boldsymbol{r})] + V_{\mathrm{ne}}[\rho(\boldsymbol{r})], \tag{6}$$

where the functional $F[\rho(\boldsymbol{r})] = T[\rho(\boldsymbol{r})] + \frac{1}{2}\int \frac{\rho(\boldsymbol{r})\rho(\boldsymbol{r}')}{|\boldsymbol{r}-\boldsymbol{r}'|} d\boldsymbol{r}d\boldsymbol{r}' + E_{xc}[\rho(\boldsymbol{r})]$, which is independent of the external field, $V_{ne}[\rho(\boldsymbol{r})]$ is the attraction potential between nuclei, $T[\rho(\boldsymbol{r})]$ is the kinetic energy of non-interacting particle models, $\frac{1}{2}\int \frac{\rho(\boldsymbol{r})\rho(\boldsymbol{r}')}{|\boldsymbol{r}-\boldsymbol{r}'|} d\boldsymbol{r}d\boldsymbol{r}'$ is the Coulombic repulsion, and $E_{xc}[\rho(\boldsymbol{r})]$ is the exchange–correlation energy functional.

However, $\rho(\boldsymbol{r})$, $\boldsymbol{T}[\rho(\boldsymbol{r})]$, and $E_{xc}[\rho(\boldsymbol{r})]$ had not been expressed in HK theorems.

Kohn–Sham Equation and Exchange–Correlation Functional

From the Kohn–Sham equation [22], $\rho(\boldsymbol{r})$ and $\boldsymbol{T}[\rho(\boldsymbol{r})]$ can be solved as shown in the following Hamiltonian:

$$\{-\nabla^2 + V_{KS}[\rho(\boldsymbol{r})]\}\varphi_i(\boldsymbol{r}) = E_i\varphi_i(\boldsymbol{r}), \tag{7}$$

where $V_{KS}[\rho(\boldsymbol{r})] = V_{ne}[\rho(\boldsymbol{r})] + V_{coul}[\rho(\boldsymbol{r})] + V_{xc}[\rho(\boldsymbol{r})]$, $V_{coul}[\rho(\boldsymbol{r})]$ is the Coulombic potential between electrons, and $V_{xc}[\rho(\boldsymbol{r})]$ is the exchange–correlation potential.

$E_{xc}[\rho(\boldsymbol{r})]$ is generally solved by the local density approximation (LDA) and the generalized gradients approximation (GGA) [23]. When the system's electron density in the space is not changed much, LDA is used to give more accurate results. Considering the uniformity of the electron density, GGA can get better energy features and more rigorous results than LDA. Now, GGA is one of the important thermotical methods employed by the first-principles and relevant researches of systemic properties. Under GGA, there are many kinds of exchange–correlation functionals, such as PW91 (Perdew–Wang) [24] and PBE (Perdew–Burke–Ernzerhof) [25]. With the development of computing power, theoretical investigation based on DFT is more and more important for the performance study of materials.

METHOD AND MODEL

Using the PW91 method with the PBE exchange–correlation functional and GGA, the electronic conductivity of $Li_{1.2-x}Na_xMn_{0.54}Ni_{0.13}Co_{0.13}O_2$ was implemented by CAmbridge Serial Total Energy Package (CASTEP) of Materials Studio 8.0, which is the quantum mechanical procedure. The plane wave pseudopotential method was used in CASTEP. The Coulombic attraction potential, between the inner layer electrons around the nucleus and those of the outer layer [26], was described by the ultrasoft pseudopotential. A plane wave cutoff was set at 440 eV. To relax all structures [27], a $4 \times 4 \times 1$ mesh of k-points in the Monkhorst–Pack scheme was taken. The self-consistency energy tolerance was 1×10^{-6} eV. To obtain the local stable structure of the material, the structure geometry should be optimized; the maximum stress tolerance, the maximum displacement tolerance, and the average force on every atom were the same as those in our previous work [19]. And DFT calculations had been carried out with the virtual mixed atom method.

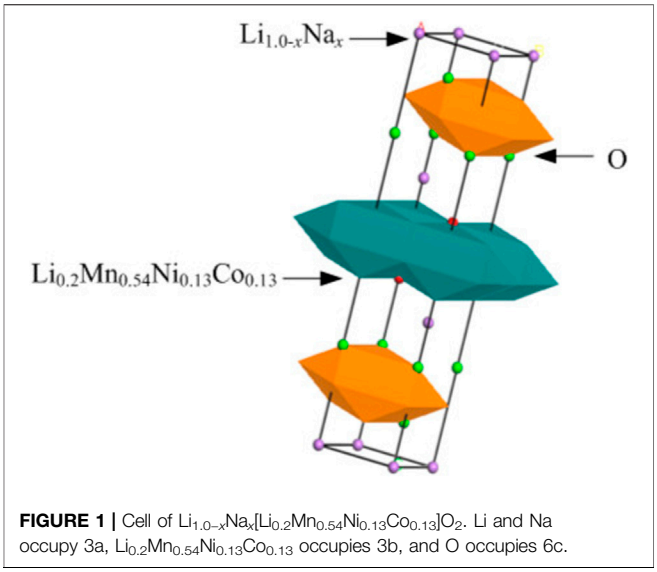

FIGURE 1 | Cell of $Li_{1.0-x}Na_x[Li_{0.2}Mn_{0.54}Ni_{0.13}Co_{0.13}]O_2$. Li and Na occupy 3a, $Li_{0.2}Mn_{0.54}Ni_{0.13}Co_{0.13}$ occupies 3b, and O occupies 6c.

The $Li_{1.0-x}Na_x[Li_{0.2}Mn_{0.54}Ni_{0.13}Co_{0.13}]O_2$ cell model is shown in **Figure 1**, and a $4 \times 3 \times 2$ supercell model was built. Li and sodium are assumed as 1.0 mol in this chemical formula; if the sodium doping amount is x mol, then Li is $1.0-x$ mol. The calculation of $Li_{1.2-x}Na_xMn_{0.54}Ni_{0.13}Co_{0.13}O_2$ (x = 0.01, 0.02, 0.03, . . . , 0.15) is analyzed as follows.

RESULTS AND DISCUSSION

Band Gap and Partial Density of States

The band gap of $Li_{1.2-x}Na_xMn_{0.54}Ni_{0.13}Co_{0.13}O_2$ is calculated, and the partial density of states (PDOS) is plotted with the sodium doping amount x = 0.01, 0.02, 0.03, . . . , 0.15 mol. The band gap and electrons in the conduction band are very important for the material's electronic conductivity. If the band gap is narrower, the conductivity of the material is better. After sodium doping, the band structure of $Li_{1.2-x}Na_xMn_{0.54}Ni_{0.13}Co_{0.13}O_2$ remains stable, but the energy gap has changed much. In **Table 1**, all band gap values are listed. **Figure 2** shows the relationship between the band gap and x. According to **Figure 2**, the band gap curve of $Li_{1.2-x}Na_xMn_{0.54}Ni_{0.13}Co_{0.13}O_2$ has three inflection points at x = 0.02 mol, x = 0.07 mol, and x = 0.12 mol, respectively, where the band gap has changed clearly. When x = 0.02 mol, the band gap value begins to decrease; at x = 0.07 mol, its value increases slightly, which may be ascribed to the expanding volume and disorder of Ni^{2+}/Li^+ cation mixing, but from then on, it decreases continually. In other words, it basically decreases with increasing x until x = 0.12 mol, which indicates sodium doping can effectively improve the conductivity of $Li_{1.2}Mn_{0.54}Ni_{0.13}Co_{0.13}O_2$ when $0.02 < x < 0.13$ mol.

The sodium doping influence on the conductivity of $Li_{1.2}Mn_{0.54}Ni_{0.13}Co_{0.13}O_2$ was achieved by the PDOS, which can clearly describe the bonding and density of states near the Fermi level. **Figure 3** shows its PDOS, respectively, when x = 0, 0.01, 0.04, and 0.10 mol. The peak of the PDOS corresponds to the electron number at this energy level. The colored lines in **Figure 3** represent

TABLE 1 | Band gap values of $Li_{1.2-x}Na_xMn_{0.54}Ni_{0.13}Co_{0.13}O_2$ with different x.

x (mol)	0	0.01	0.02	0.03	0.04	0.05	0.06	0.07
Band gap (eV)	1.577	1.573	1.574	1.536	1.479	1.423	1.364	1.429
x (mol)	0.08	0.09	0.10	0.11	0.12	0.13	0.14	0.15
Band gap (eV)	1.381	1.315	1.100	1.008	1.000	1.100	1.215	1.237

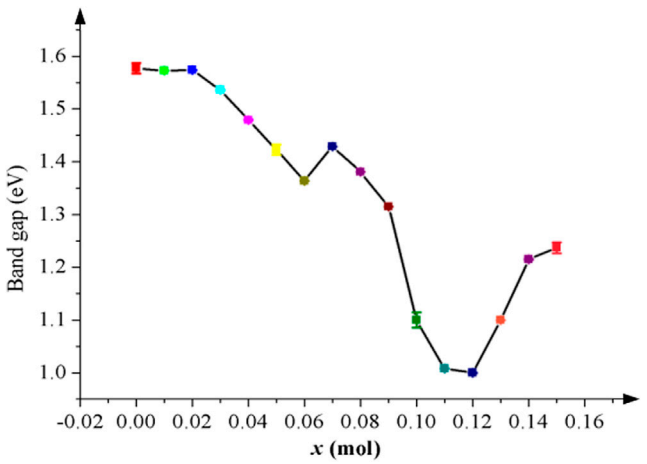

FIGURE 2 | The band gap of $Li_{1.2-x}Na_xMn_{0.54}Ni_{0.13}Co_{0.13}O_2$ becomes narrower after sodium doping, which means its conductivity is improved notably. The error bars show that the accuracy of our band gap values is reliable.

the density of different orbital states. In **Figure 3B**, when x = 0.01 mol, the PDOS peak is about 181 eV, which is subtly different from that of the pristine as shown in **Figure 3A**; when x = 0.02 ~ 0.03 mol, PDOS peaks have increased slowly; when x = 0.04 mol (shown in **Figure 3C**), the PDOS peak at the Fermi level around 201 eV may be ascribed to the wider Li–O layers made by the bigger sodium atoms' substitution, and the conductivity of $Li_{1.2}Mn_{0.54}Ni_{0.13}Co_{0.13}O_2$ is getting better distinctly; when x = 0.05 ~ 0.14 mol, the PDOS peaks have not changed much. **Figure 3D** shows the PDOS peak is about 207 eV when x = 0.10 mol; but when x = 0.15 mol, the peak of the PDOS declines. Therefore, the right amount of sodium doping can multiply greatly the electrons near the Fermi level, and sodium doping should be within x = 0.04 ~ 0.14 mol.

Cell Volume and Lithiation Formation Energy

The volume and formation energy of $Li_{1.2-x}Na_xMn_{0.54}Ni_{0.13}Co_{0.13}O_2$ were calculated. The volume data after doping indicate that x should be controlled at x < 0.11 mol. The volume is a little bigger at x = 0.07 mol than that at x = 0.06 mol; at x = 0.08 mol, it decreases again; when x > 0.10 mol, the volume expansion is huge, which will lead to the structural instability. Due to the bigger sodium atom than the lithium atom, the interslab distance of the Li–O layer can be enlarged, and the diffusion ability of Li^+ in the crystal lattice is strengthened to enhance the conductivity of $Li_{1.2}Mn_{0.54}Ni_{0.13}Co_{0.13}O_2$. More importantly, the proper sodium doping can stabilize the layered crystal structure.

It is very important to analyze the formation energy, which explicitly decides the difficulty of the lithiation/delithiation process. The greater the formation energy of metal oxide is, the higher the difficulty is for atoms to get free from the crystal lattice. The lithiation formation energy E is shown in the following equation:

$$E = E_t - E_{dl} - E_{dil}, \tag{8}$$

where E_t is the supercell's total energy, E_{dl} is the delithiation, and E_{dil} is the supercell's energy after delithiation. In **Figure 4**, the energies in **Eq. 8** are plotted to investigate the relationship between E and x. According to **Figure 4**, E has varied with x. When 0 < x < 0.09 mol, E decreases extremely, which indicates Li^+ can be deintercalated more easily and the cycling stability and rate capability of $Li_{1.2-x}Na_xMn_{0.54}Ni_{0.13}Co_{0.13}O_2$ can be continually enhanced; when 0.09 < x < 0.12 mol, E remains stable; when x = 0.10 mol, E is lowest and the rate capability is best; when x > 0.12 mol, E raises gradually. Therefore, the best doping amount x = 0.10 mol.

Electron Density Difference

To analyze the electrons' distribution near local atoms, the electron density difference of $Li_{1.2-x}Na_xMn_{0.54}Ni_{0.13}Co_{0.13}O_2$ was modulated. Compared with the pristine (**Figure 5A**), when 0 < x < 0.04 mol, the color of the electron cloud around atoms has not changed obviously and the coverage of the electron cloud is getting bigger slowly; in **Figure 5B**, the color of the electron cloud has changed much and the electron cloud's coverage is bigger significantly, which exhibit that the conductivity of $Li_{0.08}Na_{0.04}Mn_{0.54}Ni_{0.13}Co_{0.13}O_2$ is better than that when x < 0.04 mol; when x = 0.10 mol (**Figure 5C**), the color is orange and the coverage expands much, meaning that free electrons have increased enormously and its conductivity is far better than before; when x = 0.11 mol (**Figure 5D**), the color of the electron cloud is the same as that of $Li_{1.1}Na_{0.1}Mn_{0.54}Ni_{0.13}Co_{0.13}O_2$; when 0 < x < 0.14 mol, the coverage of the electron cloud is expanding continually until when x = 0.14 mol; when x > 0.14 mol, the electron cloud's coverage has shrunk a little. Therefore, sodium doping can improve the conductivity of $Li_{1.2}Mn_{0.54}Ni_{0.13}Co_{0.13}O_2$, and the excellent amount of sodium doping x = 0.05–0.13 mol.

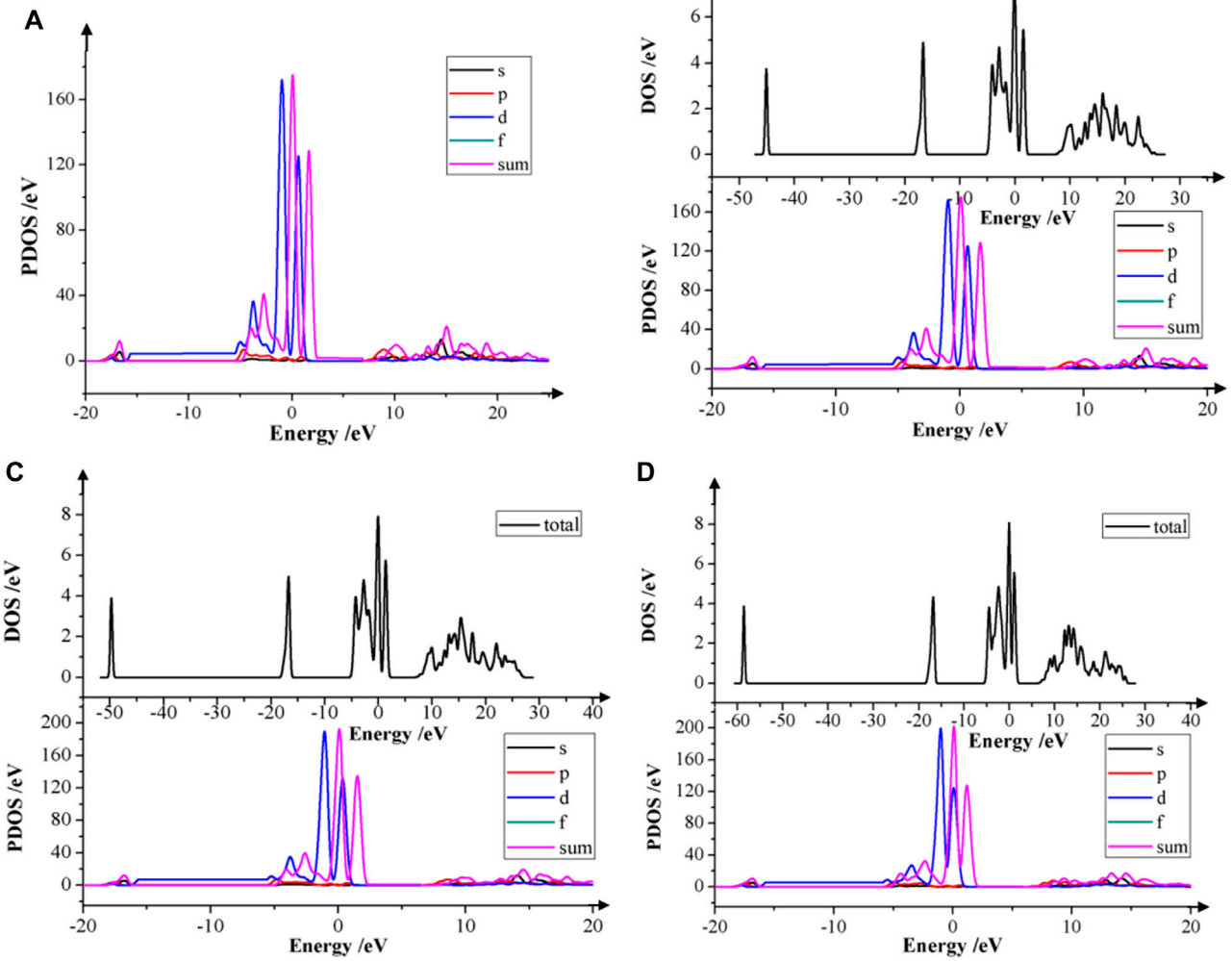

FIGURE 3 | PDOS schemas of $Li_{1.2-x}Na_xMn_{0.54}Ni_{0.13}Co_{0.13}O_2$ with different *x*. **(A)** When *x* = 0 mol, the PDOS peak of the pristine is about 173 eV. **(B)** The PDOS peak of $Li_{1.19}Na_{0.01}Mn_{0.54}Ni_{0.13}Co_{0.13}O_2$ is up to 181 eV, which is higher than that of $Li_{1.2}Mn_{0.54}Ni_{0.13}Co_{0.13}O_2$. **(C)** When *x* = 0.04 mol, the PDOS peak raises around to 201 eV. The bigger Li–O layers contribute to the better conductivity. **(D)** When *x* = 0.10 mol, the PDOS peak is approximately 207 eV, which is higher much than that of $Li_{1.2}Mn_{0.54}Ni_{0.13}Co_{0.13}O_2$.

Potential Energy of Electrons

To study the rate capability after doping, the electrons' potential energy of $Li_{1.2-x}Na_xMn_{0.54}Ni_{0.13}Co_{0.13}O_2$ had been profiled. In a potential well, if electrons have lower potential energy and get the extra external energy, they can cross freely over the potential well. In **Figure 6**, the 3D potential energy map of $Li_{1.1}Na_{0.1}Mn_{0.54}Ni_{0.13}Co_{0.13}O_2$ is shown. The different colors represent the potential energy change. In **Figure 6**, the taking turns of the potential barrier and well show $Li_{1.1}Na_{0.1}Mn_{0.54}Ni_{0.13}Co_{0.13}O_2$ is still a layered structure. And so do the potential energy maps of $Li_{1.2-x}Na_xMn_{0.54}Ni_{0.13}Co_{0.13}O_2$ when $x < 0.10$ mol, which means the right doping amount cannot lead to the phase transition.

For the purpose of investigating the sodium doping influence on the potential energy well, diffusion paths were simulated. The 2D potential energy image of $Li_{1.1}Na_{0.1}Mn_{0.54}Ni_{0.13}Co_{0.13}O_2$ is shown in **Figure 7**. Electrons will diffuse more facilely along the path marked with blue "*", which represents the minimum potential energy and can offer abundant channels to diffuse. And the energy barrier of Li^+ insertion/extraction is reduced in the crystal lattice. Therefore, electrons and Li^+ can be removed and migrated to other places almost without any energy barrier. In **Figure 7**, the potential energy of $Li_{1.1}Na_{0.1}Mn_{0.54}Ni_{0.13}Co_{0.13}O_2$ is from 36 to 1 eV, and each marked path is not the same. According to the calculations of potential energy for $Li_{1.2-x}Na_xMn_{0.54}Ni_{0.13}Co_{0.13}O_2$, the minimum potential energy decreases with rising *x*, which

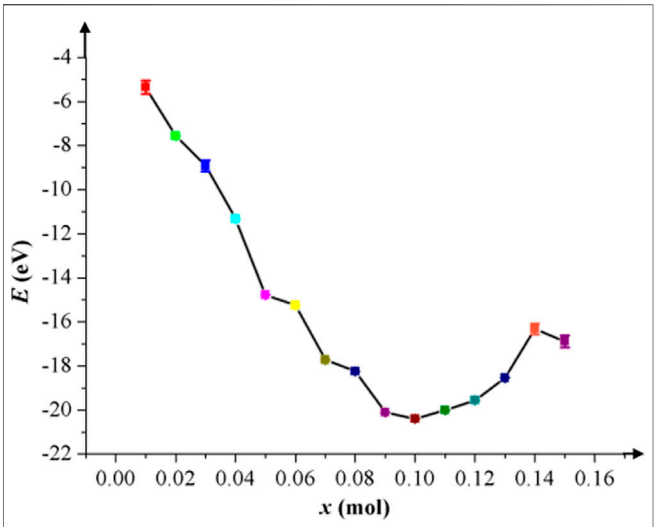

FIGURE 4 | Schematic diagram of the lithiation formation energy *E* with different *x*. The error bars show that the accuracy of our calculations is credible.

demonstrates that the potential well of $Li_{1.2-x}Na_xMn_{0.54}Ni_{0.13}Co_{0.13}O_2$ is lower, and electrons can be removed from the potential well more easily. Thus, its rate performance can be effectively promoted.

CONCLUSION

The physical and electrochemical performances of $Li_{1.2-x}Na_xMn_{0.54}Ni_{0.13}Co_{0.13}O_2$ were simulated and analyzed by DFT. The layered structure of $Li_{1.2-x}Na_xMn_{0.54}Ni_{0.13}Co_{0.13}O_2$ can be kept stably after sodium doping. According to the calculations of the band gap and PDOS, when x = 0.05–0.12 mol, $Li_{1.2-x}Na_xMn_{0.54}Ni_{0.13}Co_{0.13}O_2$ has better conductivity and cycling performance; when x < 0.11 mol, its volume remains invariable; when x = 0.10 mol, the lithiation formation energy E is lowest and Li^+ and electrons can be removed easily; based on the results of the electron density difference, when x = 0.05–0.13 mol, $Li_{1.2-x}Na_xMn_{0.54}Ni_{0.13}Co_{0.13}O_2$ has better conductivity and

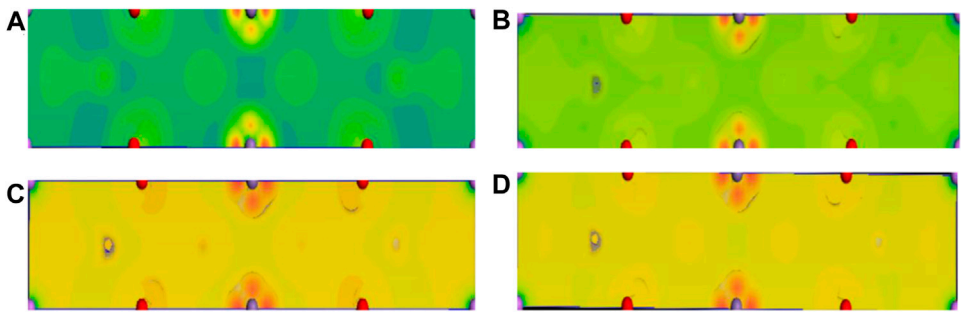

FIGURE 5 | Electron density difference of $Li_{1.2-x}Na_xMn_{0.54}Ni_{0.13}Co_{0.13}O_2$. **(A)** The electron cloud's color and coverage of the pristine are shown. **(B)** When x = 0.04 mol, the color has become orange and the electron cloud's coverage has expanded obviously, which mean its conductivity is distinguished. **(C)** When x = 0.10 mol, its color gets brighter and the electron cloud's coverage gets bigger, which indicate its conductivity is promoted extremely. **(D)** When x = 0.11 mol, there is no difference in color between x = 0.11 mol and x = 0.10 mol and the coverage of the electrons gets bigger continually.

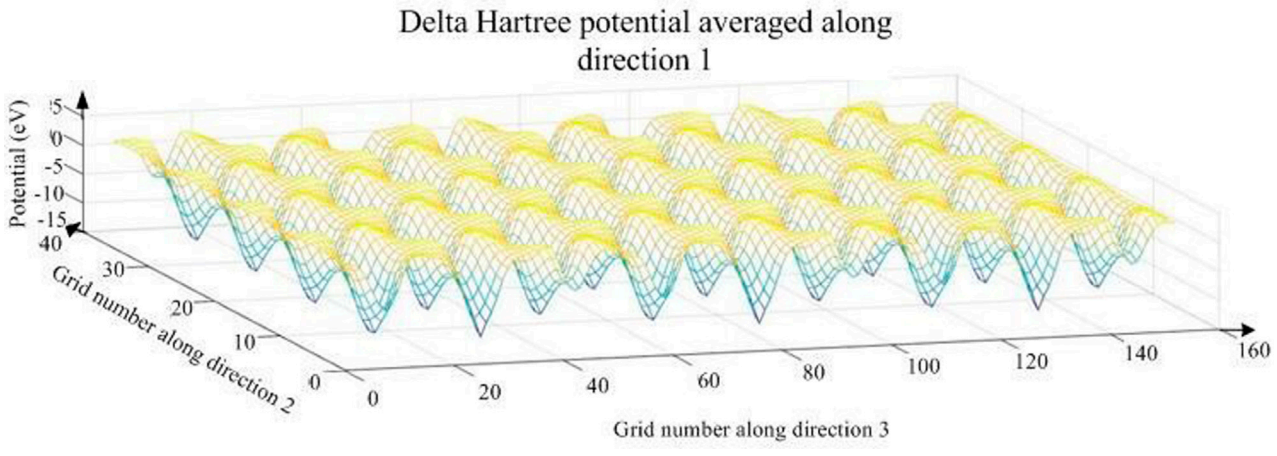

FIGURE 6 | 3D potential energy map of $Li_{1.1}Na_{0.1}Mn_{0.54}Ni_{0.13}Co_{0.13}O_2$.

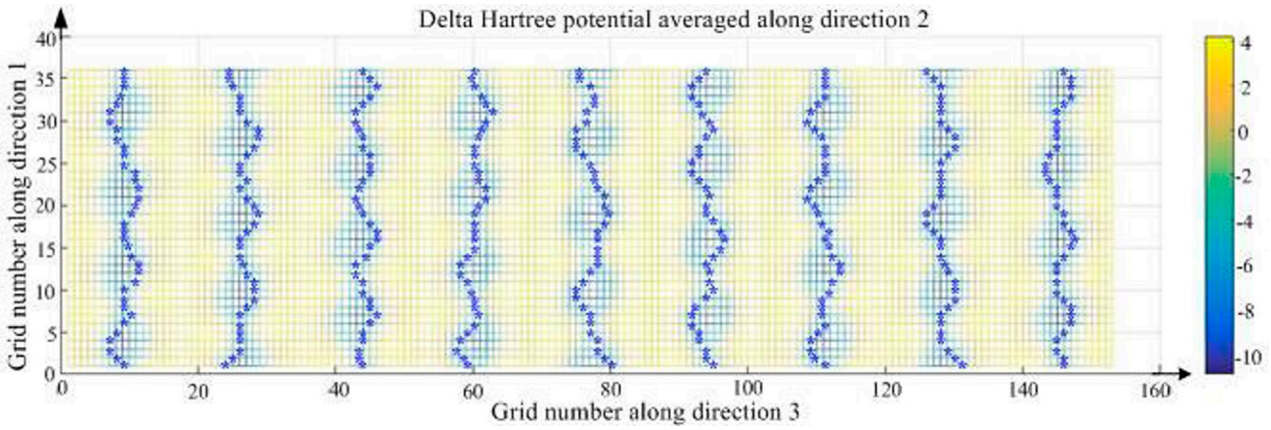

FIGURE 7 | 2D potential energy map of $Li_{1.1}Na_{0.1}Mn_{0.54}Ni_{0.13}Co_{0.13}O_2$.

electrons' potential energies are becoming lower with rising x. To sum up, when $x = 0.10$ mol, the electrochemical performance of sodium-doped $Li_{1.2}Mn_{0.54}Ni_{0.13}Co_{0.13}O_2$ is best, which is essentially in agreement with experimental results. The sample of $Li_{1.2-x}Na_xMn_{0.54}Ni_{0.13}Co_{0.13}O_2$ could be synthesized with a confinement method. Though $Li_{1.1}Na_{0.1}Mn_{0.54}Ni_{0.13}Co_{0.13}O_2$ has better electrochemical performance than $Li_{1.2}Mn_{0.54}Ni_{0.13}Co_{0.13}O_2$, other approaches should be taken as well to further improve the energy density, reversible charge capacity, and cycling performance. Our calculations, analyses, and simulations based on DFT can provide some theoretical proposals for the doping study about the electrochemical performance, and these methods can contribute to the performance study of the battery module for new electro-optical conversion devices.

DATA AVAILABILITY STATEMENT

The original contributions presented in the study are included in the article/Supplementary Material, and further inquiries can be directed to the corresponding author.

AUTHOR CONTRIBUTIONS

YG designed models, analyzed results, and wrote the manuscript. YH carried out calculations. HY gave some proposals.

FUNDING

This research was funded by the Science and Technology Project Foundation of Zhongshan City of Guangdong Province of China (no. 2018B1127), the Zhongshan Innovative Research Team Program (no. 180809162197886), the Educational Science and Technology Planning in Guangdong Province (no. 2018GXJK240), the National Natural Science Foundation of China (no. 11775047), the union project of the National Natural Science Foundation of China and Guangdong Province (no. U1601214), the Science and Technology Program of Guangzhou (no. 2019050001), and the Scientific and Technological Plan of Guangdong Province (no. 2018B050502010).

REFERENCES

1. Zhu C, Usiskin RE, Yu Y, and Maier J. The Nanoscale Circuitry of Battery Electrodes. *Science* (2017) 358(6369):eaao2808–08. doi:10.1126/science.aao2808
2. Thackeray MM, Kang S-H, Johnson CS, Vaughey JT, Benedek R, and Hackney SA. Li_2MnO_3-stabilized $LiMO_2$ (M = Mn, Ni, Co) Electrodes for Lithium-Ion Batteries. *J Mater Chem* (2007) 17(30):3112–25. doi:10.1039/B702425H
3. Song C, Feng W, Wang X, and Shi Z. Enhanced Electrochemical Performance of $Li_{1.2}Mn_{0.54}Ni_{0.13}Co_{0.13}O_2$ Cathode Material with Bamboo Essential Oil. *Ionics* (2020) 26(2):661–72. doi:10.1007/s11581-019-03233-9
4. Vivekanantha M, Senthil C, Kesavan T, Partheeban T, Navaneethan M, Senthilkumar B, et al. Reactive Template Synthesis of $Li_{1.2}Mn_{0.54}Ni_{0.13}Co_{0.13}O_2$ Nanorod Cathode for Li-Ion Batteries: Influence of Temperature over Structural and Electrochemical Properties. *Electrochimica Acta* (2019) 317:398–407. doi:10.1016/j.electacta.2019.05.095
5. Leifer N, Penki T, Nanda R, Grinblat J, Luski S, Aurbach D, et al. Linking Structure to Performance of $Li_{1.2}Mn_{0.54}Ni_{0.13}Co_{0.13}O_2$ (Li and Mn Rich NMC) Cathode Materials Synthesized by Different Methods. *Phys Chem Chem Phys* (2020) 22(16):9098–109. doi:10.1039/D0CP00400F
6. Zhang W, Liu Y, Wu J, Shao H, and Yang Y. Surface Modification of $Li_{1.2}Mn_{0.54}Ni_{0.13}Co_{0.13}O_2$ Cathode Material with Al_2O_3/SiO_2 Composite for Lithium-Ion Batteries. *J Electrochem Soc* (2019) 166(6):A863–A872. doi:10.1149/2.0171906jes
7. Luo Z, Zhou Z, He Z, Sun Z, Zheng J, and Li Y. Enhanced Electrochemical Performance of $Li_{1.2}Mn_{0.54}Ni_{0.13}Co_{0.13}O_2$ Cathode by Surface Modification Using La-Co-O Compound. *Ceramics Int* (2021) 47(2):2656–64. doi:10.1016/j.ceramint.2020.09.114
8. Liu Y, Yang Z, Li J, Niu B, Yang K, and Kang F. A Novel Surface-Heterostructured $Li_{1.2}Mn_{0.54}Ni_{0.13}Co_{0.13}O_2$@$Ce_{0.8}Sn_{0.2}O_{2-\sigma}$ Cathode Material for Li-Ion Batteries with Improved Initial Irreversible Capacity Loss Cathode Material for Li-Ion Batteries with Improved Initial Irreversible Capacity Loss. *J Mater Chem A* (2018) 6:13883–93. doi:10.1039/C8TA04568B
9. Zhou L, Liu J, Huang L, Jiang N, Zheng Q, and Lin D. Sn-doped $Li_{1.2}Mn_{0.54}Ni_{0.13}Co_{0.13}O_2$ Cathode Materials for Lithium-Ion Batteries with Enhanced Electrochemical Performance. *J Solid State Electrochem* (2017) 21(4):3467–77. doi:10.1007/s10008-017-3688-y

10. Xu L, Meng JX, Yang P, Xu H, and Zhang S. Cesium-doped Layered $Li_{1.2}Mn_{0.54}Ni_{0.13}Co_{0.13}O_2$ Cathodes with Enhanced Electrochemical Performance. *Solid State Ionics* (2021) 361:115551. doi:10.1016/j.ssi.2021.115551
11. Bao L, Yang Z, Chen L, Su Y, Lu Y, Li W, et al. The Effects of Trace Yb Doping on the Electrochemical Performance of Li-Rich Layered Oxides. *ChemSusChem* (2019) 12(10):2294–301. doi:10.1002/cssc.201900226
12. Zhang P, Zhai X, Huang H, Zhou J, Li X, He Y, et al. Synergistic Na^+ and F^- Co-doping Modification Strategy to Improve the Electrochemical Performance of Li-Rich $Li_{1.2}Mn_{0.54}Ni_{0.13}Co_{0.13}O_2$ Cathode. *Ceramics Int* (2020) 46(15):24723–36. doi:10.1016j.ceramint.2020.06.26310.1016/j.ceramint.2020.06.263
13. Liu Y, He B, Li Q, Liu H, Qiu L, Liu J, et al. Relieving Capacity Decay and Voltage Fading of $Li_{1.2}Ni_{0.13}Co_{0.13}Mn_{0.54}O_2$ by Mg^{2+} and PO_4^{3-} Dual Doping. *Mater Res Bull* (2020) 130:110923. doi:10.1016/j.materresbull.2020.110923
14. Liu Z, Zhang Z, Liu Y, Li L, and Fu S. Facile and Scalable Fabrication of K+-doped $Li_{1.2}Ni_{0.2}Co_{0.08}Mn_{0.52}O_2$ Cathode with Ultra High Capacity and Enhanced Cycling Stability for Lithium Ion Batteries. *Solid State Ionics* (2019) 332:47–54. doi:10.1016/j.ssi.2018.12.021
15. Yang C, Zhang X, Huang J, and AoZhang PG. Enhanced Rate Capability and Cycling Stability of $Li_{1.2-x}Na_xMn_{0.54}Co_{0.13}Ni_{0.13}O_2$. *Electrochimica Acta* (2016) 196:261–9. doi:10.1016/j.electacta.2016.02.18010.1016/j.electacta.2016.02.180
16. Fermi E. Eine statistische methode zur bestimmung einiger eigenschaften des atoms und ihre anwendung auf die theorie des periodischen systems der elemente. *Z Physik* (1928) 48(1):73–9. doi:10.1007/BF01351576
17. Hohenberg P, and Kohn W. Inhomogeneous Electron Gas. *Phys Rev* (1964) 136(3B):B864–B871. doi:10.1103/physrev.136.b864
18. Ng MF, and Sullivan MB. First-principles Characterization of Lithium Cobalt Pyrophosphate as a Cathode Material for Solid-State Li-Ion Batteries. *J Phys Chem C* (2019) 123(49):29623–9. doi:10.1021/acs.jpcc.9b09946
19. Gao Y, Shen K, Liu P, Liu L, Chi F, Hou X, et al. First-Principles Investigation on Electrochemical Performance of Na-Doped $LiNi_{1/3}Co_{1/3}Mn_{1/3}O_2$. *Front Phys* (2021) 8:1–8. doi:10.3389/fphy.2020.616066
20. Thomas LH. The Calculation of Atomic fields. *Math Proc Camb Phil Soc* (1927) 23:542–8. doi:10.1017/S0305004100011683
21. Jones RO, and Gunnarsson O. The Density Functional Formalism, its Applications and Prospects. *Rev Mod Phys* (1989) 61(3):689–746. doi:10.1103/RevModPhys.61.689
22. Kohn W, and Sham LJ. Self-consistent Equations Including Exchange and Correlation Effects. *Phys Rev* (1965) 140:A1133–A1138. doi:10.1103/physrev.140.a1133
23. Perdew JP, Chevary JA, Vosko SH, Jackson KA, Pederson MR, Singh DJ, et al. Atoms, Molecules, Solids, and Surfaces: Applications of the Generalized Gradient Approximation for Exchange and Correlation. *Phys Rev B* (1992) 46(11):6671–87. doi:10.1103/PhysRevB.46.6671
24. Kresse G, and Joubert D. From Ultrasoft Pseudopotentials to the Projector Augmented-Wave Method. *Phys Rev B* (1999) 59:1758–75. doi:10.1103/PhysRevB.59.1758
25. Perdew JP, Burke K, and Ernzerhof M. Generalized Gradient Approximation Made Simple. *Phys Rev Lett* (1996) 77:3865–8. doi:10.1103/PhysRevLett.77.3865
26. Vanderbilt D. Soft Self-Consistent Pseudopotentials in a Generalized Eigenvalue Formalism. *Phys Rev B* (1990) 41(11):7892–5. doi:10.1103/PhysRevB.41.7892
27. Monkhorst HJ, and Pack JD. Special Points for Brillouin-Zone Integrations. *Phys Rev B* (1976) 13:5188–92. doi:10.1103/PhysRevB.16.174810.1103/physrevb.13.5188

Conflict of Interest: The authors declare that the research was conducted in the absence of any commercial or financial relationships that could be construed as a potential conflict of interest.